Transport and Communications Science Journal, Vol. 74, Issue 7 (09/2023), 819-832

Transport and Communications Science Journal

DEVELOPMENT OF MULTI-FIBER APPROACH FINITE ELEMENT MODEL FOR REINFORCED CONCRETE BEAM USING FRP REINFORCEMENTS UNDER PURE TORSION

Nguyen Tuan Anh*, Le Dang Dung, Nguyen Xuan Huy

University of Transport and Communications, No 3 Cau Giay Street, Hanoi, Vietnam

ARTICLE INFO

TYPE: Research Article
Received: 21/08//2023
Revised: 10/09/2023
Accepted: 12/09/2023
Published online: 15/09/2023
https://doi.org/10.47869/tcsj.74.7.5

* *Corresponding author*
Email: tuananh_ktxd@utc.edu.vn ; Tel: +84946836092

Abstract. A finite element model using a multi-fiber approach is proposed in this paper for the analysis of reinforced concrete (RC) members using fiber-reinforced polymer (FRP) reinforcements, with a specific focus on the effect of pure torsion. The proposed model is formulated using a displacement-based approach and a kinematic assumption involving a two-node Timoshenko beam. The compatibility and equilibrium between concrete and FRP materials in the membrane elements are formulated based on a discretization of the cross-section into several areas following its stress state and the principle of the Modified Compression Field Theory. The nonlinear responses of RC elements with FRP bars can be predicted using an appropriate constitutive material law with internal equilibrium of transverse reinforcement and concrete. The pure torsional response is implemented using an enhanced formulation of concrete's tensile behavior, which is based on experimental tests on torsion and the characteristics of FRP materials. The good agreement between the numerical results and experimental data confirms the validity of the proposed model.

Keywords: Multi-fiber beam, FRP materials, reinforced concrete beam, pure torsion.

1. INTRODUCTION

Fiber-reinforced polymer (FRP) reinforcement has been used in civil engineering for more than two decades as an alternative to conventional steel reinforcement. Over time, many

technical reports and design codes have been published to include flexural and shear resistance [1-4]. However, there are still no guidelines or standards for torsional behavior because torsion is often considered a secondary effect to flexure and shear. This can become a big problem as torsion can be a significant and non-negligible load in structures such as spandrel and curved beams in buildings, and curved girders in bridges. If not properly considered in the design phase, torsion can lead to undesirable and brittle failure.

Design codes for torsional behavior of reinforced concrete (RC) structures are typically based on the space truss theory with fixed-angle hypothesis [5]. This theory was then developed to the variable space truss theory [6]. However, these models were proposed primarily for combined actions bending-shear-torsion. As a result, the tensile behavior of concrete in these models is always based on the stress-strain relationship obtained from shear tests. This can lead to significant differences in the modeling results of RC structures under pure torsion. To address this issue, some researchers have developed models that focus on the pure torsional behavior of RC structures. For example, a softened membrane model with a specific stress-strain relationship of concrete has been proposed [7]. Another approach is to discretize the cross-section into different regions following their stress state [8]. In addition to these analytical models, the multi-fiber approach has become increasingly popular in recent years. This approach is derived from the fiber beam-column element for earthquake-resistant response analysis of RC structures proposed by Spacone et al. [9]. The multi-fiber model has been further developed to study the pure torsion resistance of RC structures, such as some multi-fiber models using damage mechanics for the behavior of RC materials proposed by Mazars et al. [10], Capdevielle et al. [11] or Di Re et al. [12].

The limited knowledge on the torsional behavior of RC structures using FRP reinforcement is due to the lack of analytical approaches, experimental studies, and numerical models. The existing numerical and analytical models primarily focus on the strengthening and retrofitting aspect of RC structures, using space truss theory. Examples of such models include the models of Chalioris [13], Ameli et al. [14], Deifalla & Gobarah [15] or Alabdulhady et al. [16]. The torsional responses of RC elements with FRP reinforcement have also received attention from researchers, but only through analytical approaches, such as in the models developed recently by Deifalla et al. [17] or Hadhood et al. [18]. To the best of the authors' knowledge, there is currently no sectional-fiber finite element model capable of predicting the torsional behavior of RC beams using FRP bars. Experimental studies on this subject are also very limited, and most of the existing tests focus on the strengthening aspect. Therefore, the development of a numerical model and a set of experimental data is necessary to improve our understanding of the torsional behavior of FRP-reinforced concrete members.

The main objective of this study is to develop a numerical finite element model to predict the behavior of RC beams with FRP reinforcement under pure torsional effects. The model is developed from the model of Nguyen et al. [19] and considers the compatibility and equilibrium between concrete and FRP materials of membrane elements following the principle of the Modified Compression Field Theory (MCFT)-based [20] and Mohr's circle. An enhanced concrete tensile stress-strain relationship for the pure torsional response is also proposed, based on the precedent author’s work. In the case of fine-grained concrete, the compressive concrete behavior follows the instructions in the work of Nguyen Huy Cuong & Ngo Dang Quang [21]. The cross-section is discretized into different regions following their stress state, in order to take into account the tube analogy assumption of RC beams under torsion after cracking, and eventually to consider the confinement effect. The validation of the

proposed model is guaranteed by comparing the numerical results to the experimental tests and theoretical formulations available in the literature.

2. PROPOSED MODEL FORMULATION

2.1. Modelling discussion

Although the analytical approach based on space truss analogy is popular and useful for studying the torsional behavior of RC structures, numerical modeling with a sectional approach has some advantages, especially in terms of customization at the cross-section level. This allows the user to select the appropriate mechanical and material properties. This is particularly useful when considering the reduction in tensile strength of stirrups under torsional loading. In fact, many theoretical analyses and experimental results have shown that stirrups play an important role in the torsional behavior of RC components. After cracking, tensile stress is transferred from concrete to stirrup, while compressive stress in the concrete cover is transferred to the corners. The use of FRP materials, which have higher tensile strength than conventional steel, can increase torsional strength by up to 150% [17,18]. However, due to the materials properties of FRP, some researchers have reported a significant reduction in the tensile strength of composite stirrup in areas with complex stress states, such as the corner of cross-section [22]. Analytical models based on space truss analogy, which are built on the equilibrium and compatibility equations of the entire structure, cannot provide enough information to consider this reduction effect, which occurs at a local level.

The study of sectional local problems can be solved by using simulation tools provided by computational software such as ABAQUS and ATHENA. These commercial software packages offer advantages in terms of ease of use, computational speed, and consistency of results. However, they can also have limitations when solving specific problems with high order of complexity and peculiarity. For example, in the case of the torsional response of concrete structures, the tensile behavior of concrete used in analytical models and commercial software is typically obtained from shear tests. This can lead to significant differences between simulated, analytical, and experimental results. For example, a 2-fold discrepancy between the numerical and experimental values of cracking torque has been reported [7,19].

Based on the above analysis, this study proposes a numerical sectional-based model using the multi-fiber approach. The structure is divided into many longitudinal layers or fibers, and several control sections are created along the element axis. These control sections follow the Gauss-Lobatto quadrature rule for numerical integration. The intersection of longitudinal fibers and cross-section creates a system of integration points (called fiber) with their own coordinates, areas, and appropriate material law (Figure 1). The Material stresses and strains in each fiber are determined by force equilibrium or kinematic conditions. The sectional and element stiffness matrices are then computed using variational formulations and numerical integrations. The propagation of concrete crack is carried out using smeared-crack approaches, which handle cracking as a distributed effect with directionality. The Modified Compression Field Theory (MCFT) is used, along with a constitutive model to evaluate the stress-strain relationship of material points in RC members subjected to shear and axial stresses.

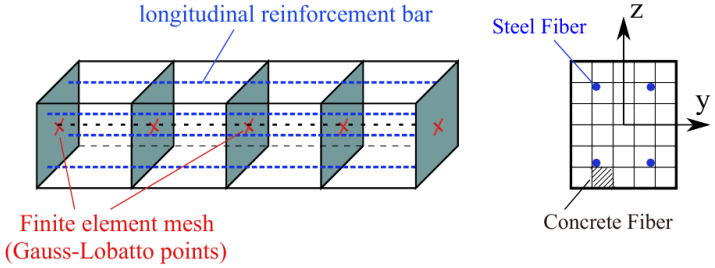

Figure 1. Multifiber approach for a RC member.

2.2. Element and sectional kinematic

Consider a two-node Timoshenko beam represented by a straight axis line delimited by end nodes I and J, and a local frame system of coordinates *(x,y,z)* as shown in Figure 2.

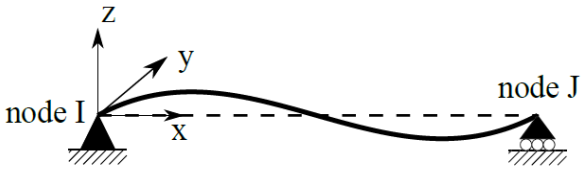

Figure 2. Two-node Timoshenko beam and the local reference system.

In general, the displacement field of a Timoshenko beams contains three translations and three rotations. However, under pure torsion, the displacement field consists in only one rotation about the longitudinal axis in every single point of the element axis. In a displacement-based formulation, this generalized displacement is determined from the nodal displacements by shape functions that are chosen linear in the present work:

$$\theta_x(x) = \frac{1-x}{L}\theta_x^I + \frac{x}{L}\theta_x^J = \begin{bmatrix} \frac{1-x}{L} & \frac{x}{L} \end{bmatrix} \begin{bmatrix} \theta_x^I \\ \theta_x^J \end{bmatrix} = \mathbf{N}_s(x)\mathbf{q}_e \tag{1}$$

where θ_x^I and θ_x^J are the twist angle at node *I* and *J* respectively; *x* is the coordinate of the section and *L* the element length; $\mathbf{q}_e$ is the vector of nodal twist angle. The twist κ_x is then equal to:

$$\kappa_x = \frac{\partial \theta_x(x)}{\partial x} = \begin{bmatrix} -\frac{1}{L} & \frac{1}{L} \end{bmatrix} \begin{bmatrix} \theta_x^I \\ \theta_x^J \end{bmatrix} \tag{2}$$

Under the hypothesis of small displacements, the kinematic relation between material displacement and twist angle is established according to Saint-Venant torsional theory in order to take in account the effect of warping. Indeed, the axial displacement is a function of the profile of warping over the cross-section and distribution of warping along the element length. In the case of a solid cross-section, the warping effect is limited, but cannot be neglected, warping is considered *free* and its distribution is constant over the element length. The displacement field of *free warping* therefore becomes:

$$\begin{aligned} U(x,y,z) &= \psi(y,z)\kappa_x \\ V(x,y,z) &= -z\theta_x(x) \\ W(x,y,z) &= y\theta_x(x) \end{aligned} \tag{3}$$

Where the term $\psi(y,z)$ represent the Saint-Venant warping function which describes the profile of warping over the cross-section, while the warping distribution is represented by the twist κ_x. The strains of any material point of the cross-section are then evaluated with only 3 components considered in the sectional analysis as follows: one normal strain and two transverse strains collected in a single strain vector $\mathbf{e}_f(y,z)$. This vector is related to the twist by a compatibility matrix containing the material point characteristic:

$$\left.\begin{aligned} \varepsilon_{xx} &= \frac{\partial U}{\partial x} = 0 \\ \gamma_{xy} &= \frac{\partial U}{\partial y} + \frac{\partial V}{\partial x} = \left(-z + \frac{\partial \psi}{\partial y}\right)\kappa_x \\ \gamma_{xz} &= \frac{\partial U}{\partial z} + \frac{\partial W}{\partial x} = \left(y + \frac{\partial \psi}{\partial z}\right)\kappa_x \end{aligned}\right\} \Rightarrow \mathbf{e}_f(y,z) = \mathbf{a}_f(y,z)\kappa_x \tag{4}$$

Once the strain vector is obtained at each fiber, an appropriate material law is applied to determine the material stresses:

$$\mathbf{s}_f = \mathbf{k}_f \mathbf{e}_f \tag{5}$$

where the $\mathbf{s}_f$ vector collect the material stresses $\begin{pmatrix}\sigma_{xx} & \tau_{xy} & \tau_{xz}\end{pmatrix}^T$, and $\mathbf{k}_f$ is the material stiffness matrix, determined by the constitutive models introduced in Section 2.3.

The torsional moment at sectional level, consequently, can be determined as an integral over the cross-section area of the stress field in the section:

$$M_{x,s}(x) = \iint_A \mathbf{a}_f^T \mathbf{s}_f \, dA = \iint_A \mathbf{a}_f^T \mathbf{k}_f \mathbf{e}_f \, dA = \mathbf{K}_s \kappa_x \tag{6}$$

$\mathbf{K}_s$ is defined as the sectional stiffness matrix. The element equilibrium is considered between internal and external potential energy, using the principle of virtual work, give the following relationship between the nodal twist angle $\mathbf{q}_e$, the external nodal torsional moment $\mathbf{M}_{x,e}$ and the external uniform torque $\mathbf{T}_u$:

$$\mathbf{K}_e \mathbf{q}_e = \mathbf{M}_{x,e} + \int_L \mathbf{N}_s^T \mathbf{T}_u \, dx \tag{7}$$

where the element stiffness matrix is defined from the sectional stiffness matrix $\mathbf{K}_s$ and the shape function matrix $\mathbf{B}_s$:

$$\mathbf{K}_e = \int_L \mathbf{B}_s^T \mathbf{K}_s \mathbf{B}_s \tag{8}$$

The model formulation was written in MATLAB, a programming language that is well-suited for handling matrix expressions. The principle of model code is general and consistent, making it easy to transform into other programming languages such as FORTRAN, C++, or Python.

2.3. Proposed material law of RC member using FRP reinforcement.

The stress-strain relationship of the FRP reinforcement is defined by its material properties. It exhibits a linear elastic behavior until failure, with the ultimate strength f_u and modulus of elasticity E_f being the most important values (Figure 3). It is important to note that in the proposed model, the ultimate strength of FRP reinforcement f_u is taken as the value of the tensile strength of FRP for shear design f_{fv}, as recommended in ACI 440.1R [1]. This tensile strength f_{fv} must be limited by the value of the strength of bent portion of FRP reinforcement f_{fb}. This is because the tensile strength of composite stirrup can be significantly reduced in areas with complex stress states, such as the corner of cross-sections [22].

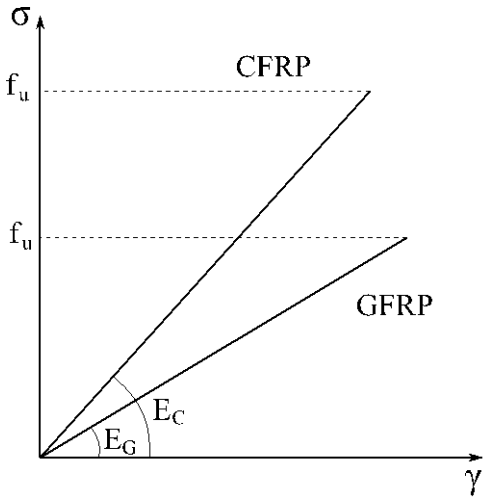

Figure 3. Behavior of FRP materials.

While the FRP constitutive law is relatively straightforward and can be evaluated in uniaxial directions, the material behavior of concrete is notably complex because it must be considered in biaxial direction. This complexity calls for a comprehensive analysis that not only encompasses torsional behavior but also includes the integration of FRP reinforcement. This context calls for the implementation of the Modified Compression Field Theory, in which the principal idea is to substitute this biaxial behavior of concrete with a uniaxial relationship. In this concept, the stress-strain is formulated in the principal direction of cracking: compressive (direction 2) and tensile direction (direction 1). Crack is assumed distributed in the concrete following a principal direction of inclined angle θ, and the principal directions of strains and stresses are assumed to be coincident. Therefore, after cracking, the diagonal concrete struts are formed, and the behavior of a free-body membrane RC member using FRP reinforcement can be considered as a superposition of concrete strut and FRP reinforcement (Figure 4).

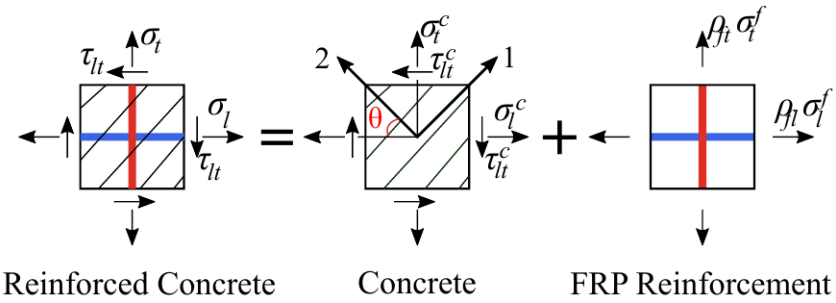

Figure 4. Equilibrium of a membrane member.

Using the principle of Mohr's circle, the principal strains and stresses are related to the crack angle, hence in an integration point (*fiber*) the direction of concrete struts can be determined. Equilibrium and compatibility equations are evaluated with the average value of the stress and strain:

$$\begin{aligned}
\varepsilon_1 &= \varepsilon_l \cos^2\theta + \varepsilon_t \sin^2\theta + \gamma_{lt} \sin\theta\cos\theta \\
\varepsilon_2 &= \varepsilon_l \sin^2\theta + \varepsilon_t \cos^2\theta - \gamma_{lt} \sin\theta\cos\theta \\
\gamma_{lt} &= 2\left(\varepsilon_1 + \varepsilon_2\right)\sin\theta\cos\theta \\
\sigma_2 \sin^2\theta - \sigma_1 \cos^2\theta + \rho_{fl}\sigma_{fl} &= 0 \\
\sigma_2 \cos^2\theta - \sigma_1 \sin^2\theta + \rho_{ft}\sigma_{ft} &= 0 \\
\tau_{lt} &= \left(\sigma_1 + \sigma_2\right)\sin\theta\cos\theta
\end{aligned} \tag{9}$$

with ε_1, ε_2 are the strains in the principal directions of concrete; θ is the angle of principal direction; σ_1, σ_2 the stresses in the principal directions of concrete; ρ_{fl} and ρ_{ft} is the FRP reinforcement ratios in longitudinal and transversal direction, respectively.

The stress-strain relationship of concrete in the principal directions is formulated in both compression and tension. In compression, it includes the softening effect of concrete since the principal compressive stress is affected by the principal tensile stress (Figure 5(a)). In tension, the stress-strain relationship aligns with the principles introduced in the constitutive model designed for RC members under torsion [19]. However, certain adaptations are made to accommodate the use of FRP reinforcement as a replacement for traditional steel (Figure 5(b)). These adaptations are proposed based on calibration, to ensure that the influence of section dimensions, reinforcements ratio as well as the simplicity of the formulation are all taken into account for the torsional behavior.

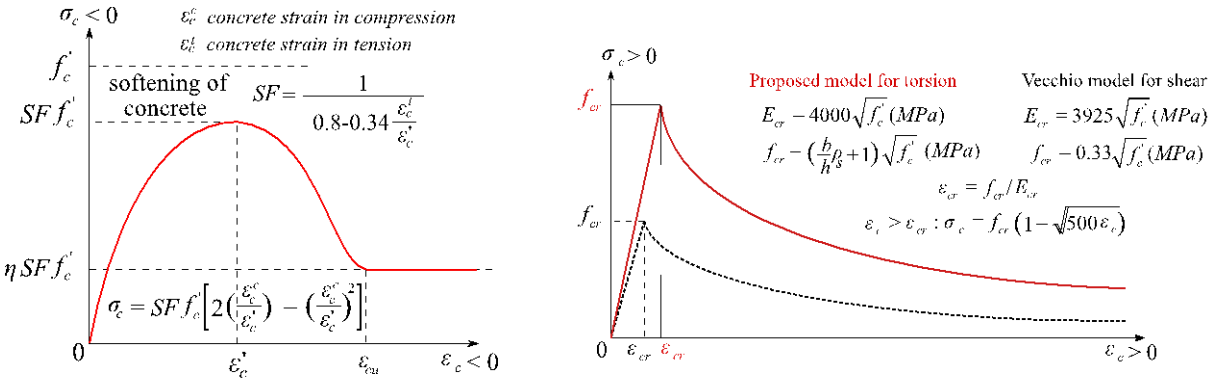

Figure 5. Concrete constitutive relationships for proposed model (case of conventional concrete).

2.4. Section discretization

A discretization of cross-section into several regions proposed by Navarro Gregori et al. [23] is borrowed in the proposed model (Figure 6). Such discretization, based on the direction of transversal reinforcement, can handle the contribution of stirrups in a multi-fiber model, by satisfying the internal equilibrium between concrete and steel. Secondly, the assumption of

tube analogy in the post-cracking phase can be realized by deactivating the contribution of the central region.

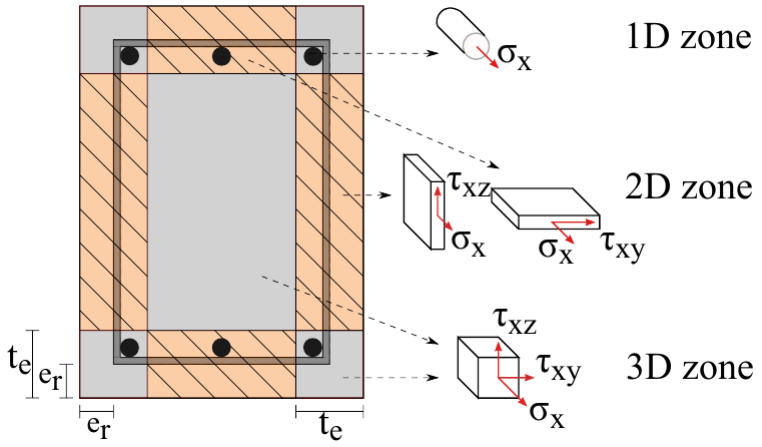

Figure 6. Discretization of cross-section following the material stress state.

The 1D-zone take into account the contribution of the longitudinal reinforcement bar (rebar) with the assumption that there is no interaction between concrete and FRP material. The only stress accounted for is the axial component σ_{xx} (or σ_l), which can be easily computed from the axial strain using an uniaxial behavior law of FRP material in Figure 3.

The 2D-zone corresponds to the portion in which the transverse FRP reinforcement crosses in one direction: vertical or horizontal. The wall thickness of the tube in the post-cracking phase is defined as the width of the 2D-zone. The stress and strain vectors in this zone are defined as $\mathbf{s}_f^{2D} = \begin{pmatrix} \sigma_l & \sigma_t & \tau_{lt} \end{pmatrix}^T$ and $\mathbf{e}_f^{2D} = \begin{pmatrix} \varepsilon_l & \varepsilon_t & \gamma_{lt} \end{pmatrix}^T$. In the strain vector, the axial term ε_l and transversal term γ_{lt} can be obtained from the sectional kinematic (expressed in Section 2.2, while the term ε_t is unknown and must be determined separately by an iteration process of satisfying the transverse equilibrium conditions at each fiber. This equilibrium condition, as defined in Eq. (9), is satisfied by imposing $\sigma_t = 0$. Consequently, the resultant stress states have two non-zero components: a normal σ_{xx} and a transversal τ_{xy} or τ_{xz} depending on the direction. The material stiffness matrix corresponds to this 2D-zone $\mathbf{k}_f^{2D}$ (in Eq. (5)) is determined based on the constitutive model in Section 2.3.

The 3D-zone corresponds to the concrete areas where transverse FRP reinforcements come across in both directions (the four corners of section) and the regions of concrete in the core of section without any reinforcement. In this context, the stress and strain states have three components: one normal σ_{xx} and two transversals τ_{xy}, τ_{xz}. The material stiffness matrix corresponds to this 3D-zone $\mathbf{k}_f^{3D}$ (in Eq. (5)) is formulated based on an extension of the original MCFT, proposed by Vecchio and Selby [24].

Detailed expressions and formulations of the material stiffness matrix, as well as the equilibrium and local transformations are available within the author's model developed for RC member subjected to pure torsion [19].

3. MODEL VALIDATION

The validity of the proposed model is confirmed by comparing its results with experimental results from the test carried out by Hadhood et al. [18] and by Le DD et al. [25]. The key aspects of the experimental setup and the subsequent numerical validation are outlined as follows.

3.1. Experimental setup

The experimental study of Hadhood et al. includes 6 specimens subjected to pure torsion, in which one beam (BGW) has no stirrup, one beam (BGST-200) has perpendicular GFRP stirrup and the last 4 beams are reinforced with GFRP spirals. In the test of Le DD et al., 7 specimens made from fine grained concrete are studied, but only 3 of them are reinforced with internal GFRP bars and stirrups (namely FRP.0, FRP.1 and FRP.2). The materials properties of FRP reinforcement and concrete are represented in Table 1. The beam and section dimensions, as well as the distribution of transverse FRP reinforcement, are shown in Figure 7 and Figure 8.

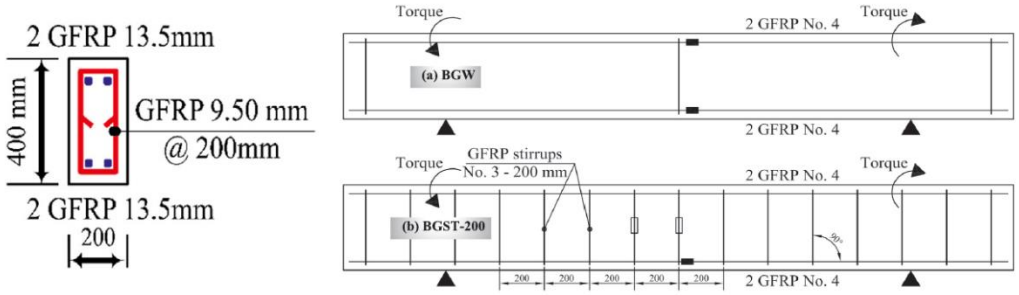

Figure 7. Details of section and reinforcement of tested beam in the experiment of Hadhood et al. [34]

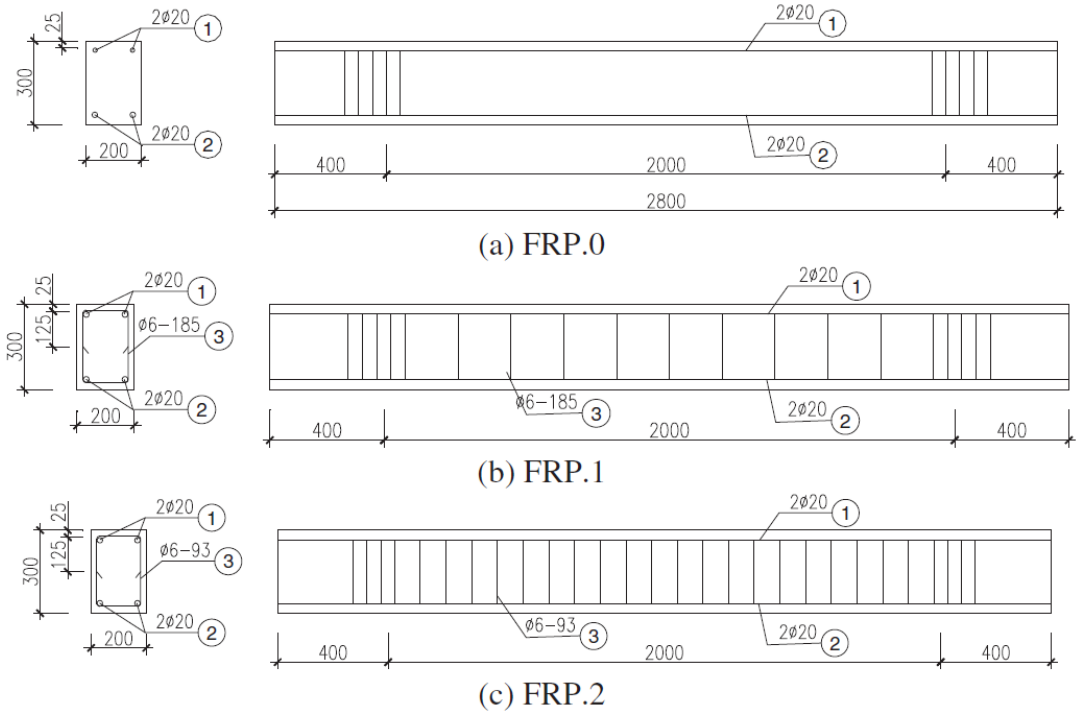

Figure 8. Details of section and reinforcement of tested beams in the reported experiment [39].

Table 1. Material properties of tested beams.

Beams	f_{ck} (MPa)	Reinforcement	E_f (GPa)	f_{fu} (MPa)	f_{fb} (MPa)	f_{fv} (MPa)	$A_{f,bar}$ (mm2)
BGW [18]	36,6	GFRP Ø9.5	44,8	950	474	179,2	70,8
BGST-200 [18]	36,6	GFRP Ø13.5	35,2	595	485	143,3	143
FRP.0 [25]	45,4	Ø6	42,5	801,3		170	19,6
FRP.1 [25]	40,7	Ø20	42,5	810		170	240,4
FRP.2 [25]	40,7						

3.2. Validation and analysis

As indicated in Table 2, the numerical results (obtained from the proposed model) are in good agreement with the experimental data. On the other hand, in the test of Le DD et al., the values of cracking torsional moment T_{cr} from the ACI 318-19 design code are significantly underestimated. The value of cracking torsional moment as defined in ACI 318-19 design code as [26]:

$$T_{cr} = \frac{\sqrt{f_c'}}{3}\left(\frac{A_{cp}^2}{p_{cp}}\right) \tag{10}$$

where A_{cp} and p_{cp} are the area enclosed by the outside perimeter and the outsider perimeter of concrete cross section, respectively. In this sequence, the analytical and experimental values of cracking torque once again showed a two-fold difference, as is the case with conventional RC beams under pure torsion [7,19]. It is also noteworthy that the analytical values of T_{cr} are the same for beams FRP.1 and FRP.2, which have the same compressive strength and section dimensions, since they are the only parameters related to the calculation of T_{cr} in not only ACI 318-19, but also other conventional design codes, such as Eurocode or CSA. In contrast, similarly to the theoretical formulation (from skew-bending theory), the proposed model has the capacity to offer reasonable and distinct T_{cr} values for each specimen, thanks to its enhanced formulation for the tensile behavior of concrete. This formulation incorporates not only concrete's compressive strength and section dimensions, but also accounts for the ratio of transverse reinforcements, which is the main different factor between the 3 tested specimens.

The torque versus twist curves of all tested beams are plotted in Figure 9, Figure 10, Figure 11 and Figure 12. The numerical values generated by the proposed model agree well with the experimental data, particularly in the pre-cracking stage. In the post-cracking stage, the proposed model also captures the significant reductions in torsional moment, as evidenced by the transition between the two phrases before and after cracking. In the case of beam BGW (Figure 9) and FRP.0 (Figure 11), which have no transverse reinforcement, brittle failures are observed in both experimental tests and the proposed model. However, the post-cracking behavior of the reinforced beams is different. For beam BGST-200 (Figure 10), the ultimate torque is higher than the cracking torque. This is consistent with the results constated in the cases of RC beams with conventional steel reinforcement, as the transverse reinforcement helps to confine the concrete and prevent it from cracking further. On the other hand, beams

FRP.1 and FRP.2, which were made of fine-grained concrete, regain some of their torsional strength after cracking, but the ultimate torque is still lower than the cracking torque: 84,4% in case of beam FRP.1 and 95,5% in case of beam FRP.2. This is because the fine-grained concrete is more brittle than conventional concrete. The proposed model captures all of these features well. After the initial drop in torque that occurs at first cracks, the beams regain some of their strength, but the ultimate torques are still lower than the cracking torques. After reaching the ultimate torque, the torsional stiffness decreases slowly, as in the experimental tests.

Table 2. Values of cracking torsional moment.

Beams	**Experimental values (kN.m)**	**Numerical values (kN.m)**	**ACI 318-19 (kN.m)**	**Skew-bending theory (kN.m)**
BGW	11,9	12,5	10,8	13,9
BGST-200	12,9	12,7	10,8	13,9
FRP.0	18,6	17,3	8,1	11,4
FRP.1	16,0	16,1	7,7	11,0
FRP.2	16,8	16,3	7,7	11,2

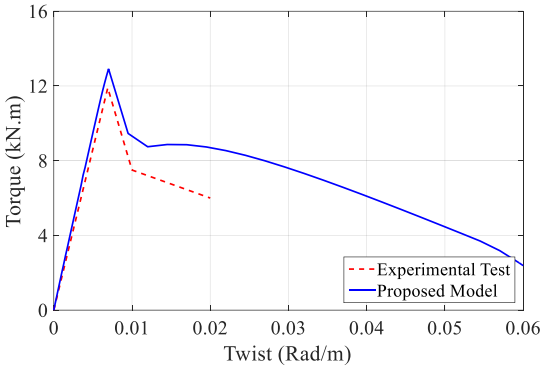

Figure 9. Torque versus twist curves of beam BGW.

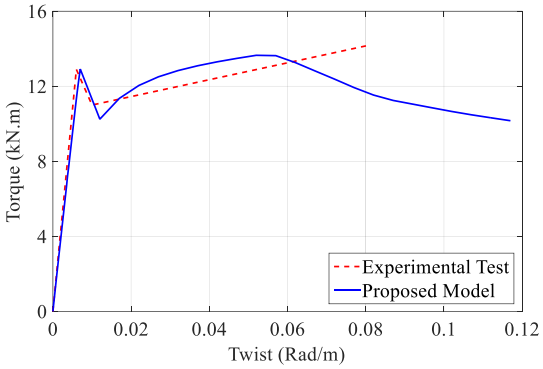

Figure 10. Torque versus twist curves of beam BGST-200.

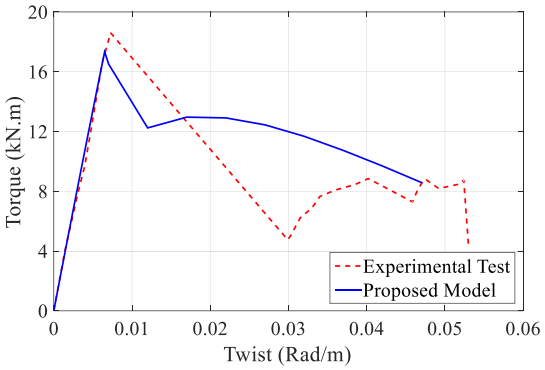

Figure 11. Torque versus twist curves of beam FRP.0

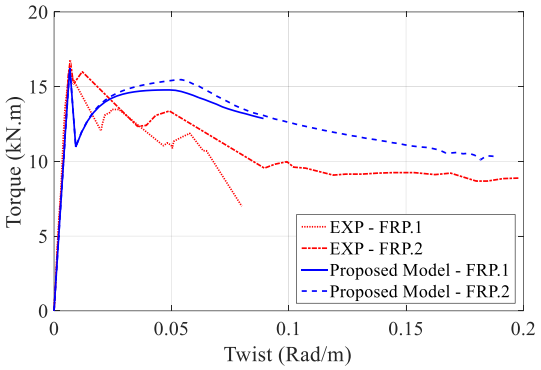

Figure 12. Torque versus twist curves of beam FRP.1 & FRP.2

4. CONCLUSION

In this study, a numerical model using a multi-fiber finite element approach is developed for RC beam with FRP reinforcement subjected to pure torsion. The element and sectional kinematics of the proposed model are general enough to be applied in any finite element model or formulation. Several numerical examples were carefully executed to demonstrate the proposed model's ability to predict the torsional behavior in the pre-cracking stage. The cracking torsional moment was accurately predicted, while the post-cracking behavior was better represented with higher torsional transverse reinforcement ratios. This is consistent with theoretical analysis.

However, the number of experimental tests in the literature is still very limited, so the consistency of the proposed model still needs to be verified. In the future, more features can be implemented in the proposed model to consider more effects such as confinement or the bond effect between concrete and FRP reinforcement.

ACKNOWLEDGMENT

This research is funded by the University of Transport and Communications (UTC) under grant number T2022-XD-011 TĐ.

REFERENCES

[1]. ACI - American Concrete Institute, State-of-the-Art report on fiber reinforced plastic (FRP) reinforcement for concrete structures, Technical Report, Committee 440 Rep. No. ACI 440R-96, American Concrete Institute, Farmington Hills, Mich, 2002.

[2]. Fib Task Group 9.3, Externally bonded FRP reinforcement for RC structures - Bulletin 14, Technical Report, International Federation for Structural Concrete (fib), 2001.

[3]. ACI - American Concrete Institute, Guide for the Design and Construction of Structural Concrete Reinforced with Fiber-Reinforced Polymer (FRP) Bars (ACI440.1 R-95), Detroit, Michigan: American Concrete Institute, 2015.

[4]. CSA - Canadian Standards, Design and Construction of Building Structures with Fibre Reinforced Polymers, 2017.

[5]. E. Raush, Design of reinforced concrete in torsion, Ph.D. thesis, Technische Hochschule, Berlin, Germany, 1929. https://doi.org/10.1061/TACEAT.0004907.

[6]. P. Lampert, B. Thurlimann, Ultimate Strength and Design of Reinforced Concrete Beams in Torsion and Bending, IABSE publications, 31 (1971) 645–655. https://doi.org/10.1007/978-3-0348-5954-7_1

[7]. C.-H. Jeng, T. Hsu, A softened membrane model for torsion in reinforced concrete members, Engineering Structures, 31 (2009) 1944–1954. https://doi.org/10.1016/j.engstruct.2009.02.038

[8]. K. Rahal, Torsional strength of reinforced concrete beams, Canadian Journal of Civil Engineering, 27 (2000) 445–453. http://dx.doi.org/10.1139/cjce-27-3-445

[9]. E. Spacone, F. Filippou, F. Taucer, Fiber beam-column model for non-linear analysis of r/c frames: Part 1. formulation, Earthquake Engineering and Structural Dynamics, 25 (1996) 711–725. https://doi.org/10.1002/(SICI)1096-9845(199607)25:7%3C711::AID-EQE576%3E3.0.CO;2-9*fib* Task Group 9.3, FRP reinforcement in RC structures - Bulletin 40, Technical Report, International Federation for Structural Concrete (fib), 2007.

[10]. J. Mazars, P. Kotronis, F. Ragueneau, G. Casaux, Using multifiber beams to account for shear and torsion: Applications to concrete structural elements, Computer Methods in Applied Mechanics

and Engineering, (2006) 7264–7281. https://doi.org/10.1016/j.cma.2005.05.053

[11].S. Capdevielle, S. Grange, F. Dufour, C. Desprez, A multifiber beam model coupling torsional warping and damage for reinforced concrete structures, European Journal of Environmental and Civil Engineering, (2015) 1–22. https://doi.org/10.1080/19648189.2015.1084384

[12].P. Di Re, D. Addessi, A mixed 3d corotational beam with cross-section warping for the analysis of damaging structures under large displacements, Meccanica, 53 (2017). https://doi.org/10.1007/s11012-017-0749-3

[13].C. E. Chalioris, Analytical model for the torsional behaviour of reinforced concrete beams retrofitted with frp materials, Engineering Structures, 29 (2007) 3263–3276. https://doi.org/10.1016/j.engstruct.2007.09.009

[14].M. Ameli, H. R. Ronagh, Analytical method for evaluating ultimate torque of frp strengthened reinforced concrete beams, Journal of Composites for Construction, 11 (2008). https://doi.org/10.1061/(ASCE)1090-0268(2007)11:4(384)

[15].A. Deifalla, A. Ghobarad, Full torsional behavior of rc beams wrapped with frp: Analytical model, Journal of Composites for Construction, 14 (2010). http://dx.doi.org/10.1061/(ASCE)CC.1943-5614.0000085

[16].M. Y. Alabdulhady, L. Sneed, Torsional strengthening of reinforced concrete beams with externally bonded composites: A state of the art review, Construction and Building Materials, 205 (2019) 148–163. http://dx.doi.org/10.1016/j.conbuildmat.2019.01.163

[17].A. Deifalla, M. Hamed, A. Saled, T. Ali, Exploring GFRP bars as reinforcement for rectangular and l-shaped beams subjected to significant torsion: An experimental study, Engineering Structures, 59 (2014) 776–786. http://dx.doi.org/10.1016/j.engstruct.2013.11.027

[18].A. Hadhood, M. G. Gouda, M. H. Agamy, H. M. Mohamed, A. Sherif, Torsion in concrete beams reinforced with GFRP spiral, Engineering Structures, 206 (2019) 110–174. https://doi.org/10.1016/j.engstruct.2020.110174

[19].T.A. Nguyen, Q.H. Nguyen, H. Somja, An enhanced finite element model for reinforced concrete members under torsion with consistent material parameters, Finite Element in Analysis and Design, 167 (2019). https://doi.org/10.1016/j.finel.2019.103323

[20].F. J. Vecchio, M. P. Collins, The modified compression-field theory for reinforced concrete elements subjected to shear, Journal of the American Concrete Institute, 83 (1986) 219–231.

[21].Nguyen Huy Cuong, Ngo Dang Quang, Experimental study on flexural behavior of prestressed and non-prestressed textile reinforced concrete plates, Transport and Communications Science Journal, 71 (2020) 37-45. https://doi.org/10.25073/tcsj.71.1.5

[22].D. Q. Ngo, H. C. Nguyen, D. L. Mai, V. H. Vu, Experimental and numerical evaluation of concentrically loaded reinforced concrete columns strengthened by carbon textile reinforced concrete jacking, Civil Engineering Journal, 6 (2020). https://doi.org/10.28991/cej-2020-03091558

[23].J. Navarro-Gregori, P. Miguel Sosa, M. Fernandez, F. Filippou, A 3d numerical model for reinforced and prestressed concrete elements subjected to combined axial, bending, shear and torsion loading, Engineering Structures, 29 (2007) 3404–3419. https://doi.org/10.1016/j.engstruct.2007.09.001

[24].R. G. Selby, F. J. Vecchio, A constitutive model for analysis of reinforced concrete solids, Canadian Journal of Civil Engineering, 24 (1997). https://doi.org/10.1139/l96-135

[25].D.D. Le, C.T.N. Tran, H.C. Nguyen, X.H. Nguyen, Torsional behavior of glass textile-reinforced concrete beams with minimum transverse reinforcements: Experimental study. Structural Concrete, 22

(2021) 3835–49. https://doi.org/10.1002/suco.202100498

[26].ACI - American Concrete Institute, Building code requirements for structural concrete, ACI 318-19, American Concrete Institute, Farmington Hills, 2019.